

Efficient subgraph-based sampling of Ising-type models with frustration

Alex Selby*

25 August, 2014

Abstract

Here is proposed a general subgraph-based method for efficiently sampling certain graphical models, typically using subgraphs of a fixed treewidth, and also a related method for finding minimum energy (ground) states. In the case of models with frustration, such as the spin glass, evidence is presented that this method can be more efficient than traditional single-site update methods.

1 Introduction

Given a graph G with a weight J_{ij} for each edge (i, j) , and variables, or *spins*, $\mathbf{S} = \{S_i = \pm 1 | i \in V\}$ for each vertex, we can consider the energy function defined by

$$H = H(\mathbf{S}) = - \sum_{\text{edges } (i,j)} J_{ij} S_i S_j.$$

Here the edges are considered to be undirected, so that if (i, j) is in the sum, then (j, i) is not. We imagine that there is frustration in the model, i.e., many small loops where the product of the weights J_{ij} is negative. This typically arises when J_{ij} is itself chosen randomly, such as in the Edwards–Anderson spin glass.

This is the most straightforward case and so convenient for descriptions and illustrations. More generally, there could be more than two possible values, or *spin states*, for S_i and there could be *external fields* — terms in $H(\mathbf{S})$ depending on individual S_i . In general, $H(\mathbf{S})$ can be the sum of arbitrary functions of the form $J_{ij}(S_i, S_j)$ and $h_i(S_i)$ for the purposes of the method described here. The empirical runs described later will involve 16 states.

Two classical problems are considered here, the first of finding **ground states** or minimum energy states, and the second of **simulating** or **sampling from** the Gibbs/Boltzmann distribution.

*alex.selby@cantab.net

Given an inverse temperature, β , the Gibbs/Boltzmann distribution over sets of spin configurations is given as usual by

$$P(\mathbf{S}) = Z(\beta)^{-1} e^{-\beta H(\mathbf{S})}, \quad \text{with} \\ Z(\beta) = \sum_{\mathbf{S}} e^{-\beta H(\mathbf{S})}.$$

Sampling from this distribution includes as a special case the problem of sampling the ground states ($\beta = \infty$), and if there is frustration then finding a ground state is known to be NP-hard for a general graph. Nevertheless, as seen in [13] and [14], ground states can be found quite efficiently for moderately large graphs by searching over a covering set of low treewidth subgraphs.

The graph property *treewidth* can be understood as the exponential complexity of using dynamic programming to compute a locally-defined quantity. More precisely, this statement applies to a graph G and a property ϕ that is a collection of functions ϕ_H for subgraphs $H \subset G$. Each ϕ_H is defined on the set of possible spin states on ∂H , the set of vertices adjacent to H but not in H . Suppose for $H \subset H' \subset G$, $\phi_{H'}(\mathbf{S}_{\partial H'})$ is equal to a simple combining function on the collection $\phi_H(\mathbf{S}_{\partial H})$, where $\mathbf{S}_{\partial H}$ ranges over the spin configurations on ∂H that are compatible with the spin configuration $\mathbf{S}_{\partial H'}$. Suppose also that there are s spin states for each vertex, there are m edges in G and the treewidth of G is w , then standard dynamic programming using the tree decomposition will compute the property ϕ_G in $O(m \cdot s^{w+1})$ steps. In what follows, we shall make use of two different choices of ϕ_H : the partition function $Z(\beta)$ for H , and a choice of random spins in H according to the Gibbs distribution.

There is a great deal of literature devoted to algorithms on families of graphs with bounded treewidth, but here it is assumed that the desired graph of study does not have bounded treewidth and the approach is to approximate it using bounded treewidth subgraphs.

The most common method of sampling Ising-type models generally involves Markov chain Monte Carlo (MCMC), updating one spin at a time according to a random process dependent on its immediate neighbours. More efficient methods using cluster updates, such as those of Swendsen–Wang or Wolff [17], are appropriate in models without frustration, but do not work well in frustrated models. The method described here uses a different cluster update method that works whether or not there is frustration.

A version of the subgraph sampling method was developed independently in 2013 by Decelle and Krzakala [3], termed belief-propagation-guided Monte Carlo sampling. The description given there apparently only considers the possibility of using trees for the covering subgraphs (and provides a method for producing such trees at random). I believe it is important to use a more general set of subgraphs, as described here, to be able to sample (or find ground states) with large and difficult models. Evidence for this is given in Section 6.

The sampling method described here is also similar to an earlier technique described by Hamze and de Freitas [6], which focuses on a Markov Random Field with observations attached. The method of [6] only considers trees for

subgraphs, and only an exact partition of the graph by trees. As shown in Section 2.1, this restriction is not necessary for the purposes of obtaining detailed balance, though under these conditions the authors manage to prove rigorous bounds showing the efficacy of their method.

The sampling method in [5] is similar to the one considered here, except that all subgraphs of a given treewidth are allowed, not just induced subgraphs. I believe this is significantly different from the method of induced subgraphs considered here and in [3], for reasons given in Section 2.

The primary method of comparison in this preprint will be wall-clock time, using a single thread on a specific reference computer (an Intel Core i7-3930K CPU running at 3.20GHz), except for the first comparison in Section 4 where the method being compared with was described by another party, and timings were not immediately available. It may seem unusual to use something platform-dependent and implementation-dependent like wall time rather than counting spin flips for example, but not all spin flips are alike and I believe it is necessary to take seriously the facts (i) that a spin flip isn't necessarily well-defined and (ii) that simpler methods are often much more easily optimised. If a simple count of spin flips were used as a basis for comparison, then this would tend to favour subgraph-based methods (at least as far as sampling is concerned, if not ground state finding). This is because conventional methods of flipping single spins can be executed efficiently without using any arithmetic operations (which is how the comparison code used here works), whereas subgraph-based sampling methods necessarily involve some kind of calculations to keep track of the Z -values.

Each comparison here will involve combining subgraph-based sampling with parallel tempering (also known as “exchange Monte Carlo”, see, e.g., [7]) and comparing this with single-site update methods also combined with parallel tempering. It is well known that parallel tempering can significantly improve performance and we apply it in both cases to ensure a useful comparison between the best available algorithms.

2 Description of sampling method

Take a collection of induced subgraphs T_1, \dots, T_m of the graph G . Recall that an induced subgraph is the restriction of G to a particular subset of vertices, and contains all the edges of G between those vertices. In other words, if both of the endpoints of an edge of G are in some T_i then the edge itself must be in T_i . We also require that $\cup T_i = G$, i.e., every vertex and edge is represented in some T_i .

We consider induced subgraphs only, as this ensures that when we sweep over a subgraph the spins of all its neighbouring vertices can be held fixed. It is possible to ignore this restriction and still use the method for a non-induced subgraph, fixing the spin value from the pre-updated graph to use as the neighbouring value during the subgraph update. However, then monotonicity would be lost: at $\beta = \infty$ an induced subgraph update is guaranteed not to increase the

global energy, but this is no longer true for non-induced subgraphs. I believe this will lead to poorer performance for non-induced subgraphs as the $\beta = \infty$ point is the most difficult and the difficulty of obtaining a ground state is a guide to the difficulty of obtaining low temperature / high β samples. The approach of [5] is to choose the best maximal subgraph of a given treewidth (not necessarily induced, so at treewidth 1 this is a spanning tree), trying to minimise the weight of the edges not in the subgraph, thereby making the approximation as good as possible.

The idea is that T_i should be chosen to be easy to solve exactly (in the sense of finding its ground states, or calculating its conditional Gibbs distribution). A good choice would be to only use subgraphs of a given treewidth. (It is not necessary to take all subgraphs of a given treewidth.) For simplicity, the examples here are all illustrated by the case of treewidth 1, i.e., T_i will all be trees, but it should be remembered that T_i will have some non-trivial treewidth w in general.

Given an induced subgraph, T , and a spin configuration, $\mathbf{S}_{G \setminus T} = \{S_i | i \in G \setminus T\}$ defined on the remainder of G , we can condition $P(\cdot)$ on $\mathbf{S}_{G \setminus T}$ to get a distribution, $P_T(\cdot | \mathbf{S}_{G \setminus T})$ over the spin configurations, $\mathbf{S}_T = \{S_i | i \in T\}$, over T .

The Monte Carlo step is to take T to be a random T_i from our fixed collection and then replace \mathbf{S}_T with a random configuration chosen according to the conditional distribution $P_T(\cdot | \mathbf{S}_{G \setminus T})$. This defines a sampling procedure, subject to the usual Monte Carlo caveats regarding burn-in and waiting for independent samples.

We need to show

- that this operation has the correct invariant distribution,
- that this operation is efficient to perform, and
- that the performance in terms of equilibration time can be better than traditional methods.

We'll take these in turn. The first two items are simple to demonstrate, but the last item is more open-ended and will be evaluated in different ways in separate sections of this preprint.

2.1 Correctness of invariant distribution

To show detailed balance, consider the flux from configuration of spins \mathbf{S} to \mathbf{S}' . Let us write $\mathbf{S}\Delta\mathbf{S}'$ to mean $\{i \in V | S_i \neq S'_i\}$. Then the flux $\mathbf{S} \rightarrow \mathbf{S}'$ is equal to

$$P(\mathbf{S}) \frac{1}{m} \sum_{T | \mathbf{S}\Delta\mathbf{S}' \subset T} P_T(\mathbf{S}'_T | \mathbf{S}_{G \setminus T}),$$

where the sum is over subgraphs in our fixed collection that include $\mathbf{S}\Delta\mathbf{S}'$. This is equal to

$$P(\mathbf{S}) \frac{1}{m} \sum_{T | \mathbf{S}\Delta\mathbf{S}' \subset T} \frac{P(\mathbf{S}')}{\sum_{\mathbf{S}'' | \mathbf{S}''_{G \setminus T} = \mathbf{S}_{G \setminus T}} P(\mathbf{S}'')}.$$

But $\mathbf{S}\Delta\mathbf{S}' \subset T$ is the same as saying $\mathbf{S}_{G \setminus T} = \mathbf{S}'_{G \setminus T}$, so the condition on \mathbf{S}'' in the sum in the denominator, $\mathbf{S}''_{G \setminus T} = \mathbf{S}_{G \setminus T}$, is equivalent to $\mathbf{S}''_{G \setminus T} = \mathbf{S}'_{G \setminus T}$, and the whole expression is thus symmetric under interchanging \mathbf{S} and \mathbf{S}' , proving detailed balance.

2.2 Efficiency of calculation

For clarity we'll scrutinise the case where the T_i all have treewidth 1, that is they are trees. In general, if T_i had treewidth w then the time taken to draw a random instance from $P_T(\cdot | \mathbf{S}_{G \setminus T})$, or to calculate $\sum_{\mathbf{S}'' | \mathbf{S}''_{G \setminus T} = \mathbf{S}_{G \setminus T}} P(\mathbf{S}'')$, would be roughly $s^{w+1} |\mathcal{E}(T, G)|$ elementary operations, where $\mathcal{E}(T, G)$ is the set of edges with at least one end in T and s is the number of (spin) states of each vertex. For illustration we show how it works with $s = 2$, $w = 1$, though results reported in later sections use up to $s = 16$, $w = 2$.

We proceed inductively over the vertices of T from its leaves inwards in the usual manner of dynamic programming based on a tree decomposition. After r steps, we have a collection, U_1, \dots, U_m of connected subtrees of T of total size $\sum_i |U_i| = r$, with $T \setminus \cup_i U_i$ being connected. For example:

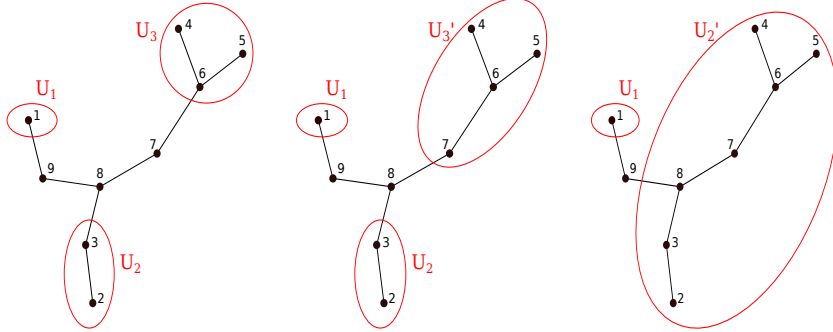


Figure 1: Three steps in the inductive evaluation and sample-choosing of a subgraph

The above vertex numbering shows one of many possible orders in which the vertices may be processed, and three successive steps are illustrated. The rule is a vertex may be processed only when at most one of its neighbours is unprocessed. Note that the rest of the graph $G \setminus T$ is suppressed in the above picture, but must be taken into account as a “background field” in the inductive calculation as it contributes to the conditional probability of the tree by interactions along edges between T and $G \setminus T$.

There are two quantities that need to be maintained inductively, for each value S_b of the boundary spins of U_i (the boundary of U_i being vertices adjacent to U_i that are not themselves in U_i ; in this tree case there is only one such vertex):

- The total Z value for U_i given S_b and $\mathbf{S}_{G \setminus T}$.

- A choice of spins of the vertices in U_i , representing a sample of the distribution $P()$ conditioned on S_b and $\mathbf{S}_{G \setminus T}$.

These two quantities are easy to maintain inductively when a vertex is added to a U_i . To illustrate the process, the example of the above pictures is traced in some detail. For U_3 in the first picture there will be, for each of the two possible values, ± 1 , of S_7

- the value Z_{U_3} defined as:

$$Z_{U_3}(S_7) = \sum_{S_4, S_5, S_6} e^{-\beta H_{U_3}(S_4, S_5, S_6, S_7, \mathbf{S}_{G \setminus T})}$$

where H_{U_3} contains the contribution to the energy from edges meeting the vertices 4, 5 and 6 of U_3 . These edges will join vertices 4, 5, 6 to each other, to vertex 7, and to $G \setminus T$, but they can't meet the other vertices of T by construction. It should be remembered that the above expression for Z_{U_3} is just a definition, not the method by which it was calculated.

- A choice of spins $\mathcal{C}_{U_3}(S_7) = (S_4, S_5, S_6)$

Moving from the first of the above pictures to the second, vertex 7 is incorporated into U_3 and 8 is the new boundary vertex. It is seen that $\Delta_H = H_{U'_3} - H_{U_3}$ only depends on S_7 and S_8 (and spins over $G \setminus T$, which we suppress), and no other vertices of T . So

- the new value $Z_{U'_3}$ is easily calculated as

$$Z_{U'_3}(S_8) = \sum_{S_7=\pm 1} e^{-\beta \Delta_H(S_7, S_8)} Z_{U_3}(S_7),$$

- and the new choice of spins is given by

$$\mathcal{C}_{U'_3}(S_8) = \begin{cases} S_7 = -1, (S_4, S_5, S_6) = \mathcal{C}_{U_3}(-1) & \text{with prob. } Z_{U'_3}(S_8)^{-1} Z_- \\ S_7 = +1, (S_4, S_5, S_6) = \mathcal{C}_{U_3}(+1) & \text{with prob. } Z_{U'_3}(S_8)^{-1} Z_+ \end{cases}$$

where Z_{\pm} are the summands in the above expression for $Z_{U'_3}(S_8)$.

When the new vertex involves fusing more than one U_i , the expression for the new Z will involve products of the old Z s. In the example above, in the transition from the second to third picture, $Z_{U'_2}$ is built up of the sum of terms of the form $e^{-\beta \Delta_H} Z_{U_2} Z_{U'_3}$.

In practice this algorithm can be easily and compactly implemented, with the spin choice being represented by a pointer. This is a small difference from the approach of [3] where a second reverse pass is used to construct the sample values for the spins of the subgraph (which will be a tree). Some care is needed for a fast implementation since straightforward methods of dealing with the inevitable large numerical range of values involve computing logarithms and exponentials

and generating random numbers in the inner loop, or the loop one level outside it, which would be rather slow. These can be avoided, for example by using look-up tables for the exponentials, rescaling the Z -values when necessary, and storing and judiciously reusing random numbers. See Appendix B for further discussion of numerical aspects. The code used to produce the results below is available from [12].

3 Chimera graphs

Experiments in this preprint were carried out on Chimera graphs ([4], [2]) of various sizes. These were chosen because originally the aim was to compare ([13], [15]) classical optimisation with that of D-Wave hardware [2] — a quantum device whose current implementation is based on a Chimera graph. This preprint will not contain any comparisons against D-Wave hardware as its aim is look at classical optimisation and simulation techniques in their own right.

An $n \times n$ Chimera graph, C_n , consists of $8n^2$ vertices arranged as n^2 complete bipartite graphs $K_{4,4}$. We shall use the notation $N = 8n^2$ throughout. Writing the bipartite decomposition of $K_{4,4}$ as $A \cup B$, the n^2 graphs of the form A are pointwise connected horizontally in rows, and the graphs of the form B connected vertically. An 8×8 Chimera graph is illustrated in Fig. 2. The separate 4-vertex A and B graphs can be thought of as “**big vertices**” (a term used throughout this preprint) in a simpler collapsed graph with $2n^2$ vertices.

The Chimera graph is highly non-planar in that its genus is at least $(4/3)n^2 + O(n)$, which follows from the fact that the complete graph K_{4n+1} can be minor-embedded into C_n . This means that matching techniques [1] that enable ground states of planar, and by extension low genus, graphs to be found in polynomial time are not applicable here. On the other hand, while the Chimera graph is not simply two dimensional, it isn’t fully three dimensional either. In [9] it is shown that in a certain scaling limit, C_n behaves like a planar graph in that it has no positive critical temperature. This result is apparently at odds with the fact that K_{4n+1} is minor-embeddable in C_n and should have a positive critical temperature because a complete graph is effectively infinite dimensional. However, these facts can be reconciled because $|K_{4n+1}|/|C_n| \sim \sqrt{2/N}$ and [9] is not concerned with features on the scale of $1/\sqrt{N}$. Furthermore [9] considers a uniform weight distribution on the edges of C_n which would not translate to a uniform weight distribution on the edges of K_{4n+1} .

The treewidth of C_n is $4n$, or n in terms of big vertices. In practice, C_n can be exhaustively searched using a simple treewidth-based method to find either ground states or perfect Gibbs samples at inverse temperature β , for n up to 8 on a normal desktop computer. Larger sizes rapidly present problems in terms of memory as well as time for this method. It is possible that branch-and-cut methods could be combined with heuristic methods to increase beyond $n = 8$ the largest C_n that can be exhaustively searched, but that is not explored here.

Following [11], the class of random instances **Range r** is defined by choosing each edge coupling randomly from the set $\{-r, -r + 1, \dots, -1, 1, \dots, r\}$. The

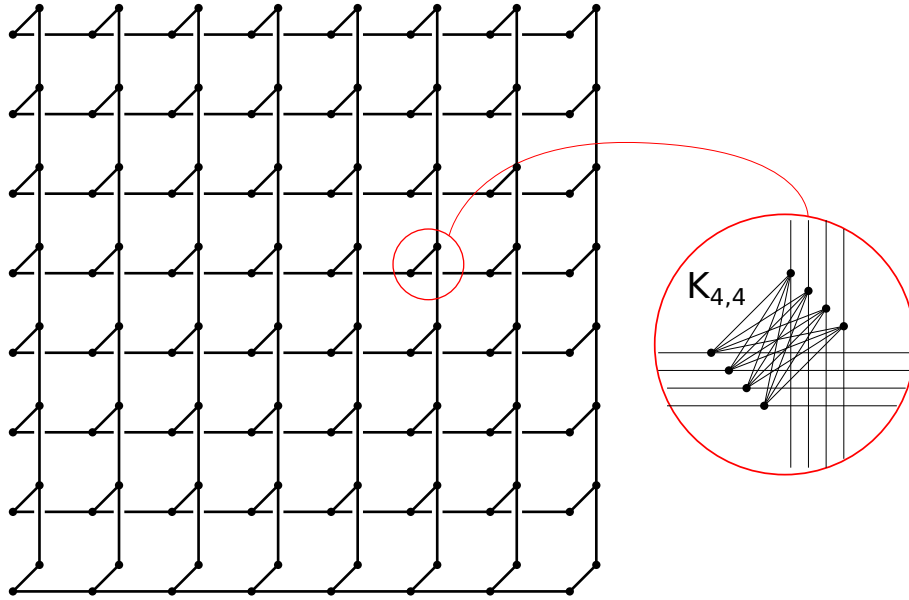


Figure 2: 8×8 Chimera graph shown in collapsed view with 128 “big vertices”, the inset showing a portion of the full 512-vertex graph

instances considered here are Range 1 in Section 4 and Range 7 in other sections.

4 Comparison - equilibration time and Binder ratio

In [9] the authors study, inter alia, the critical behaviour of bimodal ($J_{ij} = \pm 1$, same as Range 1) spin-glass on the Chimera graph. They make a prediction for its universality class, and test this by showing that the expectation of the Binder ratio as a function of suitably-scaled temperature is independent of the size N of the underlying graph (figure 2, upper, of [9]).

This gives us an opportunity to compare the subgraph-based sampling methods described here with the more standard, though well-tuned, Monte Carlo methods used in the paper.

There are now two levels of probability space: the space of random J_{ij} (known as the “disorder”), and for a given choice of J_{ij} , the space of spins, \mathbf{S} (averaging over which can be referred to as taking a “thermal average”).

In [9], parallel tempering is used, which greatly improves convergence in this sort of problem. It is a kind of Monte Carlo meta-method and can be used “on top” of another Monte Carlo method. [9] uses a standard Monte Carlo sweep as the subroutine. For comparison we also use parallel tempering, but instead base it on top of subgraph-based sampling.

The comparison we examine is with $p = 0.5$, $N = 512$ in the notation of [9]. That is, the graph is the Chimera graph of order 8 and J_{ij} are IID ± 1 . (For avoidance of doubt, it is assumed here that the Hamiltonian given there in formula (1) as $-\sum_{i,j=1}^N J_{ij} S_i S_j$ was intended as $-\sum_{i < j} J_{ij} S_i S_j$, otherwise the undirected edge weights $J_{ij} + J_{ji}$ would effectively be taken from the set $\{-1, 0, 1\}$, not $\{-1, 1\}$ as they are meant to be.)

The choice of temperatures used here covers a similar range (0.2 - 2) to that specified in table 1 of [9] (0.212 - 1.632). The temperature choice here was decided upon by trying to make the exchange probabilities between adjacent temperatures in the parallel tempering method all equal to 0.6, which ended up requiring 25 temperatures for the range 0.2 - 2. (As it turned out, these probabilities got a little higher than that for the bottom two temperatures. In retrospect, this exchange probability of 0.6 may have been a bit higher than optimal.)

For a given disorder, [9] takes two independent random spin configurations, \mathbf{S} and \mathbf{S}' and defines the spin overlap $q = (1/N) \sum_i S_i S'_i$. Then the quantity of interest is its excess kurtosis, the Binder ratio

$$g_q = \frac{1}{2} \left(3 - \frac{\langle q^4 \rangle}{\langle q^2 \rangle^2} \right)$$

Here $\langle . \rangle$ denotes thermal average and disorder average. The interest is in the thermal average, as it is trivial to sample J_{ij} to obtain the disorder average.

At very low temperatures, assuming the ground state is close to unique, we might expect q to take the values close to $+1$ or -1 according to whether \mathbf{S}' happened to hit the same ground state as \mathbf{S} or its negation. This would make g_q close to 1. At high temperatures, S_i will be independently ± 1 , which makes

$q \approx 2(1/N)B(N, 1/2) - 1 \approx N(0, 1/N)$ and so $g_q \approx 0$. This is what we see, with g_q apparently decreasing smoothly at intermediate temperatures indicating the lack of a phase transition at $T > 0$, at least in the scaling limit as $N \rightarrow \infty$.

The subgraph-based method used here in this experiment was the Gibbs analogue of the method known as strategy 3 in Appendix B of [13] and as PT-TW1 in Sections 5 and 6. It uses the collapsed Chimera graph of 128 aggregate vertices with 16 spin states each, and there is a prescribed set of 32 trees.

The relevant question in this simulation is how many steps the Monte Carlo process takes to equilibrate, i.e., for the associated Markov chain to reach something close to an equilibrium distribution. For each disorder, a pair of spin states is initialised uniformly at random at each temperature. Then R exchange parallel tempering steps are performed, which involves R tree-steps for each temperature. At that point the states are deemed to be in thermal equilibrium and they are run for R further Monte Carlo steps during which the thermal averages $\langle q^2 \rangle$ and $\langle q^4 \rangle$ are evaluated.

This whole process (including disorder average) was repeated for increasing values of R , (250, 500, 1000, 2000, ...) until the final values of g_q appeared to stabilise within acceptable error margins (up to 0.01 absolute). It turned out this required $R = 1000$, i.e., 1000 tree-steps. As far as I can gather, in terms of elementary operations, such a tree-step should be approximately comparable to about 100 standard Monte Carlo sweeps, when both are optimised, making about 100,000 sweep-equivalents for equilibration. This compares with the 2^{21} , or about 2,000,000 sweeps required in [9], so it appears there might be a significant advantage with this approach; but see also the discussion below.

The graph in Fig. 3 shows the results of the method described here applied to the bimodal (Range 1) example problem of [9] with $N = 512$. The graph in Fig. 4 shows the errors artificially amplified by a factor of 10, since they are too small to be seen clearly at their true scale. As can be seen, there is good agreement with the results given in Fig. 2 of [9], with similar uncertainties. In both cases the results are averages over 5964 disorders. These graphs serve as a check that the method described here is functioning correctly. They do not compare performance, because that is hidden in the number of equilibration steps required for each disorder.

Returning to the performance comparison, as alluded to above, there are some problems with this comparison. In particular, we are making the following assumptions:

- that there is an equivalence between sweeps and tree-steps
- that the accuracy (used as a termination criterion) is comparable
- that the parallel tempering algorithms are tuned in the same way, or if not, that the impact of any differences is negligible

The next sections describe how we have attempted to construct new comparisons that compare the two approaches on as fair a basis as possible.

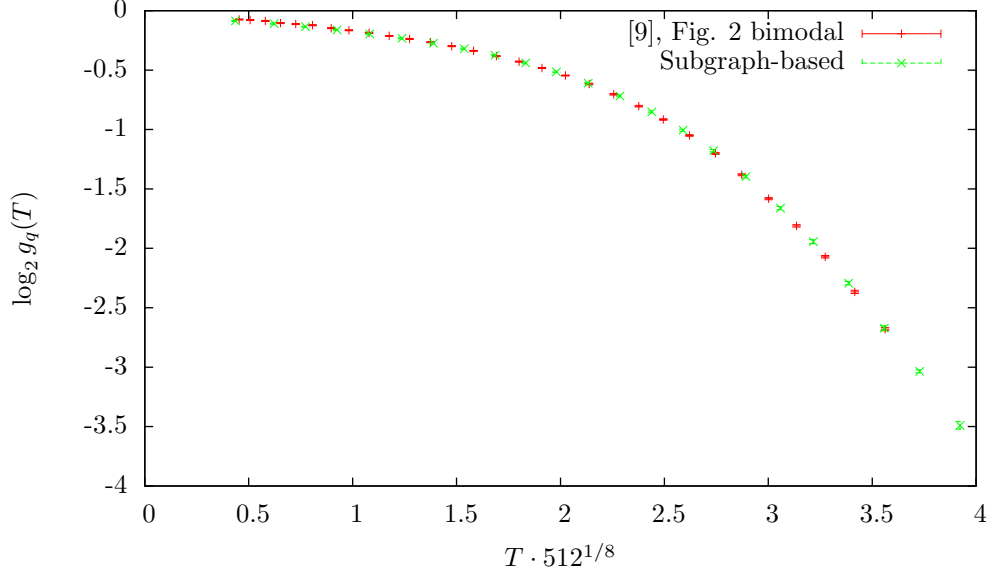


Figure 3: Log Binder ratio vs rescaled temperature at $N=512$ after 5964 anneals
— comparison with [9].

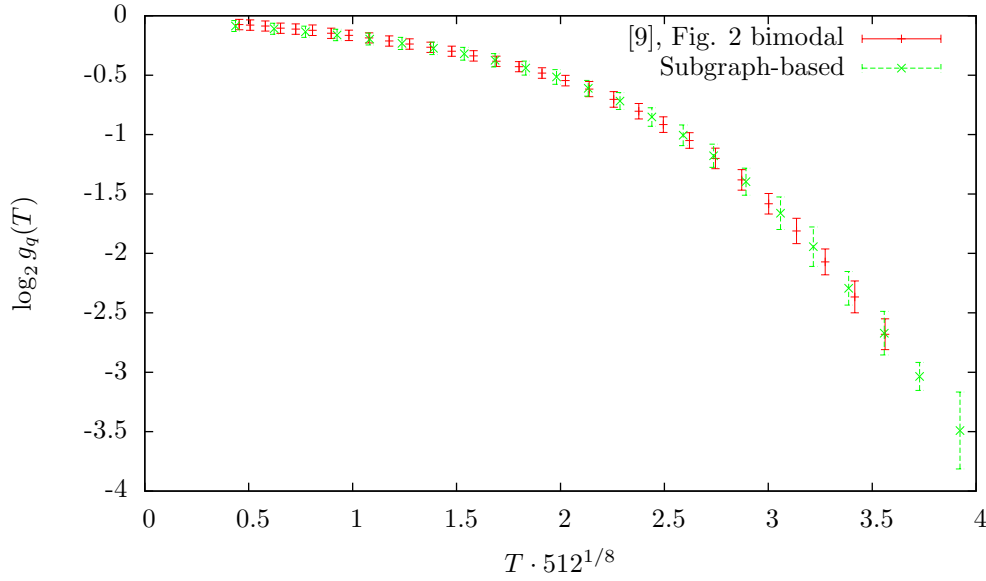


Figure 4: Log Binder ratio vs rescaled temperature at $N=512$ after 5964 anneals
— errors multiplied by 10.

5 Comparison of equilibration time using ground state values as the termination criterion

To make a much more careful and controlled comparison of subgraph-update-based sampling with site-update-based sampling, we choose a particular problem, and try to simulate it using versions of these two methods that are as nearly identical as possible. As a matter of notation:

- **SGS** shall mean subgraph-update-based sampling in general, as described in Section 2. In the example below, we shall consider **PT-TW1**, parallel tempering using treewidth 1 in the “big vertex” graph.
- **SSS** shall mean single-site-update-based sampling. In other words, the traditional method whereby each spin variable is updated depending only on its immediate neighbours. (To be clear, this category includes multispin methods, such as that described in [8]. Even though these methods operate on more than one spin at a time, the outcome is the same as operating on spins individually.) The comparison below will use **PT-TW0**, parallel tempering using a conventional update based on immediate neighbours, in terms of big vertices.

The particular problem set chosen is that of the Chimera graphs of sizes 6×6 , 8×8 , 10×10 and 12×12 (number of spins 288, 512, 800 and 1152 respectively). For these graphs, the couplings on the edges are chosen uniformly from the 14 possibilities $\pm 1, \pm 2, \dots, \pm 7$, there are no external fields and each spin can be $+1$ or -1 . This mimics the “Range 7” (harder) example set from [11].

In fact the J_{ij} used were half the values stated above, i.e., chosen from $\pm \frac{1}{2}, \pm \frac{2}{2}, \dots, \pm \frac{7}{2}$, so that the energy quantum, the smallest possible change in energy due to a change in S_i for a given disorder J_{ij} , is 1 rather than 2. Of course this scaling factor doesn’t fundamentally change anything because β can always be rescaled, but we state it explicitly to allow the reader to interpret the numbers in what follows, where we mention specific values of β and maximum allowable absolute errors in energy.

To make an interesting and fair comparison we would ideally compare the best SGS-based method against the best SSS-based method, in so far as that makes sense. Of course, we don’t necessarily know the best methods, but parallel tempering currently stands out as one of the best methods known for equilibration of such frustrated models.

5.1 Parallel Tempering parameters

For each problem size, (6×6 , 8×8 , 10×10 and 12×12), we choose 100 random disorders, and for each of these we determine the time required for the SGS- and SSS-based methods to equilibrate to a reasonable accuracy. The principal

statistic comparing SGS with SSS is simply the respective totals of these times, though other comparisons may be considered.

It may be argued that fixing the required accuracy for each disorder does not match the likely underlying objective, which is to get a good expectation over disorders. It may be, for example, that it is more efficient to spend less time trying to equilibrate the most difficult disorders, allowing them to be less accurate, on the grounds that they will be compensated for by the majority of more accurate disorders. I do not believe this kind of optimisation technique would help a great deal for two reasons. First, by the nature of the exponential decay of the subleading eigenvalue of the Monte Carlo iteration, there should be a fairly sharp change from an inaccurate result to an accurate one as the number of equilibration steps crosses the characteristic threshold for that particular disorder. That means that one can't afford to use much less than the proper number of equilibration steps, otherwise the results would be very inaccurate and swamp the accurate results from other disorders. Second, scrutinising the results here, though there are certain disorders that are considerably harder than the others, these still don't represent an overwhelming proportion of the total equilibration steps expended over all 100 disorders.

The set of temperatures is determined by fixing an effective absolute zero at $\beta = \beta^* = 20$ and aiming for a constant transition acceptance rate, 0.25, between neighbouring β s. The value $\beta = 20$ is sufficiently large (for the class of disorders considered here) that there is only a negligible chance of a state at this inverse temperature not being the ground state. [10] describes such a constant acceptance rate as in general “not too bad, but not optimal”. The temperature set here is determined in advance of the actual simulation using a method based on the average energy and heat capacity at a range of different temperatures. The acceptance rates during actual simulations match the target value reasonably well, almost always lying between 0.2 and 0.3.

Having fixed the maximum β , and having fixed the spacing between the β s by deciding on the transition acceptance rate, the remaining parameter to be decided is the minimum β , or equivalently the number of temperatures. This is determined by trying a range of different possible values on a trial set of disorders and seeing which number of temperatures requires the fewest steps on average to equilibrate. It is found that SGS requires slightly fewer temperatures than SSS for a given problem size, thus SSS will end up with some “bonus information” about high temperature states. However, it is not given credit for this, and all that is compared is the time required to estimate the ground state energy (and so presumably low temperature states) to a given accuracy. The justification for this is that it is assumed that the main interest lies in colder temperatures (strong coupling, high β), since higher temperatures are relatively easy to simulate using any sensible method. Full details of the sets of temperatures used are in Appendix A.

5.2 Determination of Equilibration

Equilibration is determined using the following method. Starting from a set of uniformly random states at each temperature, n Monte Carlo steps are performed. Each such step consists of doing a single-temperature step at each temperature and then attempting to perform exchanges. After that, n more steps are performed during which any observables can be measured and the energy at β^* is averaged to make a sample value E_1 . This whole process is repeated 25 times starting each time from random initial states, and the average value $E = (E_1 + \dots + E_{25})/25$ is formed. If this is within a chosen threshold (taken to be 0.2 here) of the smallest energy observed at any point so far, E_{\min} , then it is deemed that n steps are sufficient for equilibration. (It is possible to simultaneously test, for each m , whether the smaller number of steps m would have sufficed in not much more time than it takes just to test n itself.)

This procedure relies on a number of assumptions. First, that E_{\min} is the true ground state energy. Empirical evidence strongly suggests that it is, but for the purposes of comparison it may not matter too much if it isn't, provided that the same value of E_{\min} is used for both SSS and SGS, and this can be checked. Second that β^* is the hardest value of β to equilibrate and the states at other temperatures will have equilibrated if the state at β^* has. Even if this turns out not to be an accurate assumption, then at least SSS and SGS are still being compared on an equal basis. In any case, it is assumed that the lower temperatures are the objects of interest and the higher temperatures are a means to this end. The third assumption is that the number of restarts (25) is sufficiently large to get a good estimate of the required number of equilibration steps. The number 25 was chosen to limit the total computer time for all experiments to a week or so, but in fact it is on the small side and there is a noticeable variance in the estimate for the required number of equilibration steps. However, when the estimate is averaged over 100 disorders, this variance becomes tolerably small.

5.3 Timing

The aim is to compare wall time, though for practical reasons we break this down into the product of the number of parallel tempering (PT) steps and the time per PT-step. A PT-step includes a sweep at each temperature and the attempting to do an exchange for each pair of neighbouring temperatures. The time for such a step is liable to change if low-level spin-flip algorithms are optimised, if the computing device changes, or if there are other processes running on the computer. Separating out the wall time into a platform-independent step count and a simple low-level timing frees us up to do the step-counting runs in any environment with code at different stages of optimisation, means that we only have to measure the timings once under controlled conditions, and enables us to consider the effects of further optimisations. It is hoped that the ratio $t_{\text{PT-TW1}}/t_{\text{PT-TW0}}$ of times per step for the respective methods is fairly robust and won't vary too much across different platforms, though it is a significant

assumption that this ratio is stable under further optimisation of the respective low-level spin-flip algorithms. The times t_{TW1} and t_{TW0} were measured on a reference computer (an Intel Core i7-3930K CPU @ 3.20GHz) where both spin-flip algorithms (TW1, TW0) underwent a similar degree of effort in optimisation. They work in an analogous way as far as it makes sense for them to do so. TW0 is optimised further in the following way, eliminating all arithmetic operations for a given β , it only requires a simple lookup of the neighbours of a spin to get the probability that the new spin should be up or down, whereas for TW1 it appears to be actually necessary to accumulate Z-values. The arithmetic involved in TW1 can, however, be reduced to a few simple multiplications, additions and divisions, with no exponentials or logarithms necessary in the inner loops, due to a fortunate way in which the required numerical range is locally bounded: see Appendix B for further details. The level of optimisation used here is not as great as with the fastest multispin implementations described in [8], though the code is general enough to work just as well with arbitrary weights J_{ij} . In the language of [8], the TW0 code used here achieves about 0.16 spin-flips per nanosecond using a single thread.

The timings for the implementation and computer used are given in Appendix A.

5.4 Results of equilibration comparison

Chimera size	N	n_{TW0}	$t_{\text{TW0}}^{\text{eq}}/\text{s}$	n_{TW1}	$t_{\text{TW1}}^{\text{eq}}/\text{s}$	$t_{\text{TW0}}^{\text{eq}}/t_{\text{TW1}}^{\text{eq}}$
6×6	288	3.76×10^3	0.0549	68.5	0.0126	4.36
8×8	512	2.24×10^4	0.804	303	0.136	5.91
10×10	800	1.49×10^5	10.7	1.24×10^3	1.26	8.44
12×12	1152	6.00×10^5	85.8	3.25×10^3	6.05	14.2

Table 1: Results. n_{TW0} and n_{TW1} denote the number of equilibration steps required, and the last column gives the time advantage of TW1 over TW0.

Table 1 shows a modest but potentially useful speed improvement (last column) which appears to increase with problem size. The factor of 14 is small enough that it could potentially be erased by a better implementation of TW0, but on the face of it it is worth having, and may increase for larger problem sizes.

6 Comparison - finding ground states using parallel tempering

Four methods are compared here, named GS-TW1, GS-TW2, PT-TW0 and PT-TW1. GS-TW1 and GS-TW2 are specialised ground state finding algorithms described in Appendix B of [13] (where GS-TW1 corresponds to strategies 3 and

13, and GS-TW2 corresponds to strategies 4 and 14) and reviewed in subsection 6.1 below, using treewidth 1 and 2 subgraph neighbourhoods respectively as measured in big vertices, roughly equivalent to treewidth 4 and 8 in terms of single spins (though slightly more powerful than that, due to handling half of the $K_{4,4}$ as a single unit).

PT-TW0 and PT-TW1 are parallel tempering each with a fixed set of temperatures (for each graph size), where the Monte Carlo move updates, respectively, the spin variables of a subgraph of treewidth 0 (conventional update based on immediate neighbours) or one of treewidth 1 (tree-based Monte Carlo move as described in Section 2). The treewidths 0 and 1 are in terms of big vertices and are roughly equivalent to treewidths 0 and 4 in terms of single spins (though, as before, slightly more powerful than that).

6.1 Ground state finding method GS-TW w ($w = 0, 1, 2, \dots$)

This is the basic method we use to search for low energy states or ground states, subject to adjustments as noted below. $E(S)$ denotes the energy of state S . As noted above, treewidth w refers to big vertices, so is approximately equivalent to treewidth $4w$ on individual spins.

1. Set $A = \{\}$, a multiset, and randomise the current state (configuration of spin variables), \mathbf{S} .
2. Randomly perturb \mathbf{S} and let $B = 0$.
3. Let $E_0 = E(\mathbf{S})$. Repeatedly loop through each subgraph in the treewidth w subgraph collection and change \mathbf{S} by performing subgraph updates at $\beta = \infty$ until you've done a sweep that doesn't lower the energy. Let $E = E(\mathbf{S})$.
4. If $E < E_0$ then let $A = A \cup \{E\}$, $B = 0$.
5. Increase B by $|\{a \in A | a \leq E\}|$. If $B/|A|$ is below a certain threshold then go back to step 3, otherwise go to step 2.

It is worth remembering that even at $\beta = \infty$ (finding the minimum energy of the subgraph) the subgraph update is random because it has to make choices between equal energy substates as it runs.

The subgraph collections used are fixed and chosen by hand, as illustrated in Appendix C.

The idea of the B counter is that $|\{a \in A | a \leq E\}|/|A|$ approximates the probability, p , that a random state being considered has lower energy than the current one, and the above method tries to spend time proportional to $1/p$ considering states which are p of the way up the energy distribution. In that way, it tries to spend a longer time working on the more promising states.

This is an idealised non-terminating version of the algorithm, finding lower and lower energies indefinitely. The time-to-solve (TTS) of GS-TW w is defined by the average time it takes this version to find the ground state energy, as if

there is an oracle that knows the answer and can halt the solver when it has found it. The solver is not required to state any particular level of confidence in its answer, only to arrive at it.

In practice, the above algorithm is modified to terminate at or below some target energy E_t . It is then called with successively lower values of E_t , each time returning the lowest energy found. The timing evaluator then looks something like this:

1. Let $E_t = \infty$
2. Let $n = 0$, timer = 0
3. Repeat until $n = 500$:
4. Call above algorithm, modified to terminate at or below energy E_t .
 Let E be the minimum energy obtained during this run.
5. If $E < E_t$, let $E_t = E$ and goto step 2
6. Let $n = n + 1$
7. Result is n instances of energy E_t found in the time interval T since timer was last set to 0, and the estimated TTS is T/n .

The random number generator is never reset, so that runs should be independent. If the final energy obtained is E_{\min} , then a state with energy E_{\min} will have been encountered $n + 1$ times during the process. The first occurrence has to be discarded for timing purposes since it was obtained before it was known that E_{\min} was the minimum energy, and so runs were being interrupted and restarted.

Waiting for 500 minimum energy states serves two purposes. First, it makes the estimated TTS more accurate, both statistically and also by overcoming the accuracy limitations of the CPU timer on the computer for fast cases. Second, it allows one to be reasonably confident that it has found the actual ground state rather than just a low energy state. Experimentally it appears that the energy landscape is sufficiently well-behaved that during the course of using the above algorithm to look for an energy $E > E_0$, where E_0 is the ground state energy, there is a reasonable probability (at least 0.05 or so for Range 7, and usually much lower) that it will encounter an energy less than E , and these probabilities are independent for different runs. This means that finding 500 independent minimum energies should ensure that there is only a small chance $0.95^{500} \approx 7 \times 10^{-12}$ of having missed the true ground state. Of course this is by no means a rigorous argument and there remains the possibility of hidden bad cases arising with larger n . However, this regularity hypothesis has been verified for $n \leq 8$ where exact ground states can be found, and for $n > 8$ it is at least still valid to compare the various solvers by requiring each to find the same lowest energy state found by any of the solvers.

6.2 Results of ground state finding

The comparison was made on Range 7 instances, which are harder and perhaps better for comparison purposes than Range 1 instances as they don't have a large artificial degeneracy. GS-TW1 and GS-TW2 were run for $n = 4, 5, \dots, 16$. For $n < 10$, 1000 instances were used; for $n = 10$ and $n = 11$, 500 instances were used; for $n = 12$ and $n = 13$, 250 instances were used; and for $n > 13$, 100 instances were used. PT-TW0 and PT-TW1 were run for even values of n from 4 to 16 inclusive. For $n < 10$, 1000 instances were used; for $n = 12$, 250 instances were used; and for $n > 12$, 100 instances were used.

The results are shown in Fig. 5. The graphs of log-time vs linear size are approximately linear (though perhaps slightly concave) with different gradients in each case. PT-TW1 outperforms PT-TW0 by some margin, and the gap appears to widen with problem size. Interestingly, PT-TW1 crosses over GS-TW1, showing the effectiveness of parallel tempering as a meta-technique. GS-TW2 is initially worse than GS-TW1 for the easier problems, but crosses over at approximately $n = 13$ ($N = 1352$), showing the value of using moderately high treewidth (GS-TW2 has a treewidth of 8 in terms of individual spins).

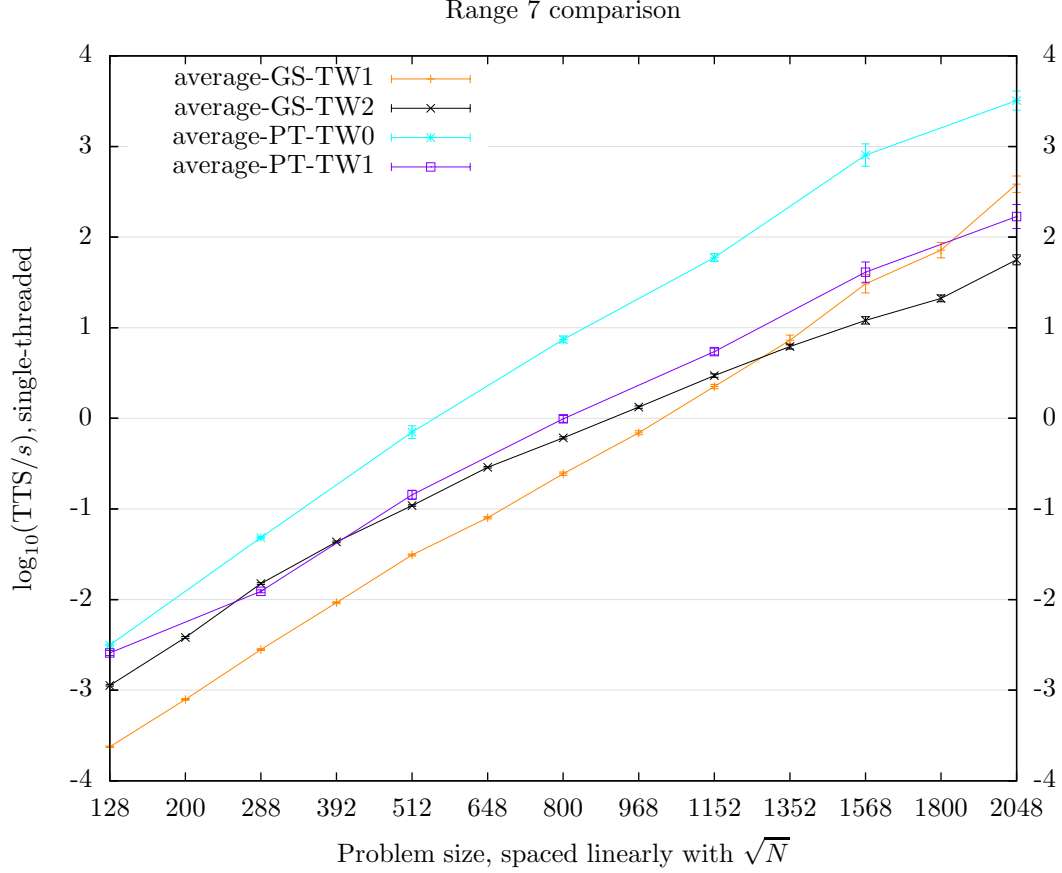


Figure 5: Comparison of four methods of finding ground states

7 Conclusions and discussion

The above results show some evidence for an advantage of using subgraph-based methods over traditional spin-flip methods, and also some evidence that this advantage increases with problem size. The question arises as to how representative these results are of more general problems on more general graphs.

It is possible that a constant factor of this advantage could be erased by improvements to the low-level SSS spin-flip, such as using a GPU, that might not be applicable to the SGS case. On the other hand, if the problem were generalised slightly, for example by using more than two spin states, then the extra complexity may hit SSS harder than SGS.

It is possible that a dynamically adaptive method of choosing temperatures, as mentioned in [10], would help SSS more than SGS, because it might be especially helpful with the difficult disorders for which SGS has a greater advantage

over SSS. It is hard to make a confident guess at the differential advantage, and so this needs to be tested.

On the other hand, the Chimera graph is in fact a relatively easy graph to simulate because it is somewhat sparse and locally-connected. Since the advantage of SGS over SSS appears to be larger with the more difficult disorders and larger problem sizes, it is possible that a more difficult graph altogether would show the advantage of SGS over SSS considerably more strongly, though this can't be taken for granted as the subgraphs used would also become more restricted. An interesting next experiment would be to see how well SGS methods, using different treewidths, perform on a 3D spin glass.

It would be interesting to apply the methods described here to Markov Random Fields, possibly giving more efficient inference in certain difficult cases. This was the motivating factor in [6] and [5].

Appendices

A Further details of equilibration comparison

Chimera size	β s used by SSS only	β s used by SSS and SGS
6×6	0.256 0.296 0.346	0.414 0.507 0.645 0.882 1.375 2.598 20.000
8×8	0.285 0.322	0.363 0.414 0.478 0.559 0.669 0.840 1.121 1.646 2.894 20.000
10×10	0.310	0.341 0.376 0.419 0.472 0.539 0.622 0.736 0.892 1.134 1.531 2.222 3.507 6.166 20.000
12×12	0.250 0.269 0.289	0.310 0.337 0.367 0.399 0.439 0.489 0.552 0.630 0.727 0.850 1.018 1.264 1.626 2.169 3.110 4.850 20.000
14×14	0.244 0.259 0.275 0.292 0.310	0.333 0.358 0.385 0.419 0.455 0.495 0.545 0.608 0.677 0.763 0.871 1.006 1.190 1.442 1.812 2.417 3.724 20.000

Table 2: Temperature sets used

Chimera size	N	$t_{\text{SSS}}/\mu\text{s}$	nt_{SSS}	$t_{\text{SGS}}/\mu\text{s}$	nt_{SGS}	$t_{\text{SGS}}/t_{\text{SSS}}$
6×6	288	14.6	10	184	7	12.6
8×8	512	35.9	12	449	10	12.5
10×10	800	71.7	15	1020	14	14.2
12×12	1152	143	20	1860	17	13.0
14×14	1568	229	23	2800	18	12.2

Table 3: Setup and low-level reference timings. nt_X is the number of temperatures used for method X .

B Numerical considerations

Given the basic method of Section 2 to compute the Z -values of the partial subgraphs, there are still a number of ways of implementing it. If the values of $\log(Z)$ are stored instead of Z then it will be necessary to perform logarithms and exponentials in the inner loop, which will be slow. (It would not be possible, in all but the simplest cases, to use look-up tables to eliminate this, since the number of entries in such a table would be exponential in the number of neighbouring vertices of the subgraph.)

Instead of storing $\log(Z)$, the implementation here stores the Z -values themselves. This means that it is possible to avoid all logarithms and exponentials in the inner loop by using a look-up table of $e^{-\beta n}$ for the relatively manageable number of different β s and n arising from energy differences from a single vertex. (A slight enhancement is to use look-up tables to precalculate values of n arising from a small neighbourhood of a vertex, rather than from the single vertex itself.) Using Z -values in this way is quite convenient and means that the inner loop calculation involves only a few lookups, multiplications and additions. However, there is a potential problem that the values of Z can become too large or small for a particular floating point representation. For speed, one would ideally like to be able to use a native representation, typically IEEE 754 binary64 (double) or 80-bit extended precision format native to the x86 processor family.

Recall from Section 2, sampling a spin configuration on a subgraph T proceeds by constructing intermediate partition functions, $Z_H(\mathbf{S}_{\partial H})$, of a series of subgraphs $H \subset T$. The partition function $Z_H(\mathbf{S}_{\partial H})$ depends on the spin configuration on ∂H , where ∂H is the “boundary within T ”, the set of vertices of T adjacent to H that are not in H (and also on $\mathbf{S}_{G \setminus T}$, though this latter dependency is suppressed as $\mathbf{S}_{G \setminus T}$ is constant during the sampling process associated with T). The question arises: how much precision (size of mantissa) and range (size of exponent) is required to store $Z_H(\mathbf{S}_{\partial H})$ adequately?

The precision presents no problem because all Z -values are *positive*-linear combinations of other Z -values. At each stage of the algorithm a random choice of spins will be made based on the relative values of $Z_H(\mathbf{S}_{\partial H})$, that is the spin configuration $\mathbf{S}_{\partial H}$ is chosen with probability $Z_H(\mathbf{S}_{\partial H}) / \sum_{\mathbf{S}'_{\partial H}} Z_H(\mathbf{S}'_{\partial H})$. Thus to make an accurate random choice, it is sufficient to know $Z_H(\mathbf{S}_{\partial H})$ to

a modest relative accuracy of, say, 10^{-9} . Because these Z -values are positive-linear combinations of other Z -values from other subgraphs, it is sufficient to know these other Z -values to a relative accuracy of 10^{-9} .

Turning to the required size of the exponent of the floating point representation, we first observe that the overall normalisation of the Z -values doesn't matter. That is, $Z_H(\mathbf{S}_{\partial H})$ can be multiplied by an overall factor λ_H , depending on H but not on $\mathbf{S}_{\partial H}$. This means that we are not worried if all of the Z -values simultaneously become very large or small as H grows. However, on the face of it, it is possible that for a given H the relative values for different spin configurations, $Z_H(\mathbf{S}_{\partial H})/Z_H(\mathbf{S}'_{\partial H})$, might be too big or small, which would present a problem no matter how the Z -values were rescaled.

Fortunately at this point we are rescued by a convenient fact. The range of Z -values for a given H is limited by construction to a locally-computable constant and does not grow with the size of the partial subgraph it is defined on.

To see this, let us first define $E(\mathbf{S}_H)$ to be the total energy of the spin configuration \mathbf{S}_H taken along edges within H and along edges between H and $G \setminus T$, and $E(\mathbf{S}_{\partial H}; \mathbf{S}_H)$ to be the total energy of the spin configurations $\mathbf{S}_{\partial H}$ and \mathbf{S}_H taken along edges joining ∂H to $H \cup \partial H \cup (G \setminus T)$. Then

$$Z_H(\mathbf{S}_{\partial H}) = \sum_{\mathbf{S}_H} e^{-\beta(E(\mathbf{S}_H) + E(\mathbf{S}_{\partial H}; \mathbf{S}_H))}.$$

If $M(H)$ is defined by

$$M(H) = \max_{\mathbf{S}_H, \mathbf{S}_{\partial H}, \mathbf{S}'_{\partial H}} |E(\mathbf{S}_{\partial H}; \mathbf{S}_H) - E(\mathbf{S}'_{\partial H}; \mathbf{S}_H)|,$$

then for two different boundary spin configurations $\mathbf{S}_{\partial H}$ and $\mathbf{S}'_{\partial H}$, we have

$$e^{-\beta M(H)} \leq Z(\mathbf{S}'_{\partial H})/Z(\mathbf{S}_{\partial H}) \leq e^{\beta M(H)}.$$

Note also that $E(\mathbf{S}_{\partial H}; \mathbf{S}_H) = E(\mathbf{S}_{\partial H}; \mathbf{S}_{H \cap \partial \partial H})$, so $E(\mathbf{S}_{\partial H}; \mathbf{S}_H)$ does not notice what goes on deep within H . The choice of subgraphs will typically be designed to minimise the boundary ∂H , and for the examples of T in this preprint, $M(H)$ is defined by a local calculation involving only a few vertices.

The maximum β that can safely be used with this simple floating point representation of Z is determined by the maximum value of $M(H)$ over subgraphs H of T that are used in the tree decomposition, the maximum degree of a node in the tree decomposition and the size of the exponent in the floating point representation. The actual calculations of $M(H)$ are quite tedious and omitted here, but in the examples used in this preprint it was found that by using extended precision floating point representation, β^* (the largest inverse temperature that it was necessary to use; see Section 5.1) was comfortably smaller than the maximum value of β not causing calculations to overflow.

C Subgraphs used for GS-TW1 and GS-TW2

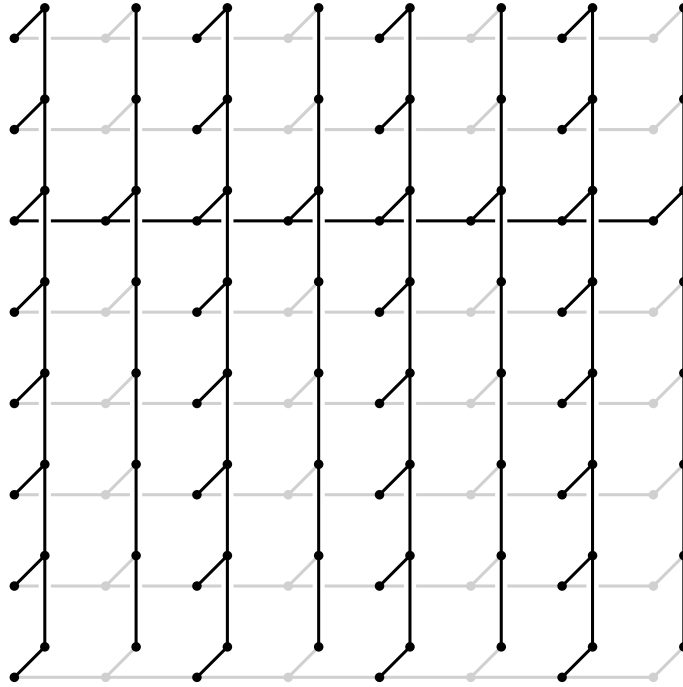


Figure 6: A maximal induced tree (shown in dark) on the “big vertex” graph used for method GS-TW1. Including the versions of this subgraph with horizontals exchanged for verticals, there are 32 possible sets of this form. Coverage = $100/128 = 78.1\%$ of “big vertices”.

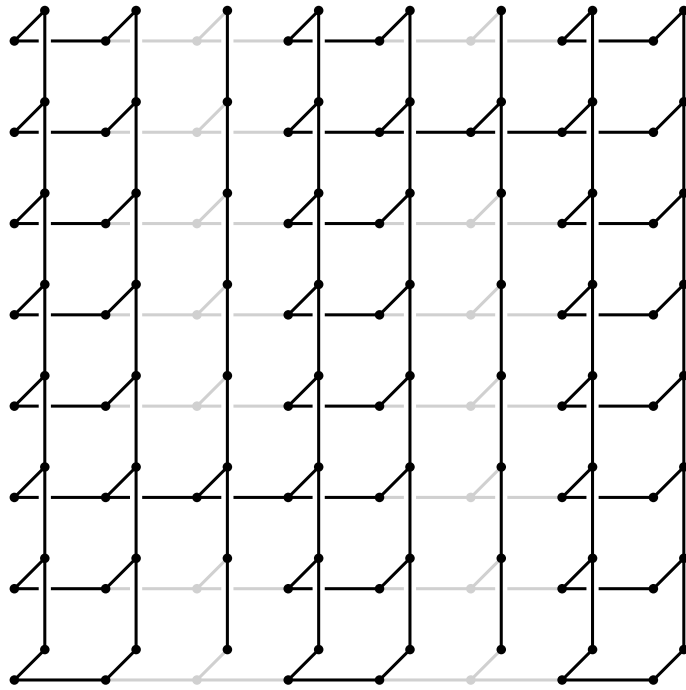


Figure 7: A maximal induced treewidth-2 subgraph used for method GS-TW2. Coverage = $114/128 = 89.1\%$ of “big vertices”.

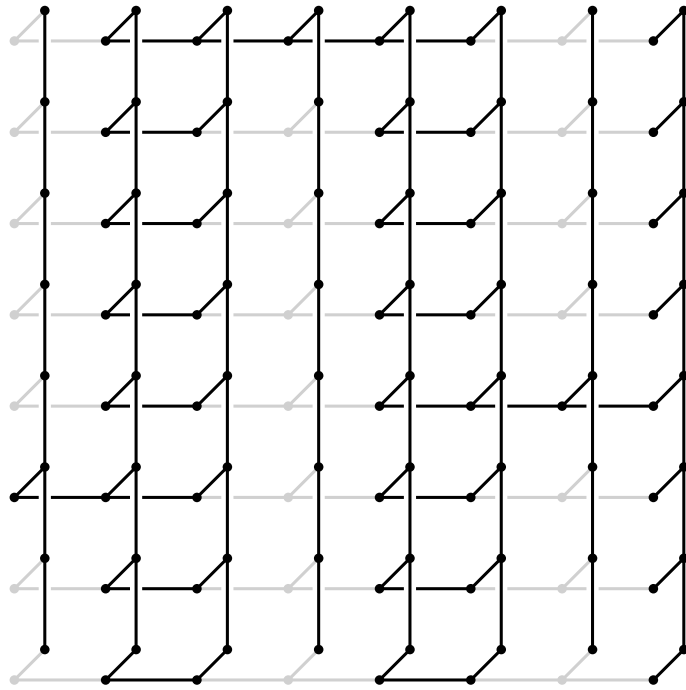


Figure 8: Another maximal induced treewidth-2 subgraph used for method GS-TW2. Coverage = $107/128 = 83.6\%$ of “big vertices”.

References

- [1] L. Bieche, R. Maynard, R. Rammal, and J.P. Uhry. On the ground states of the frustration model of a spin glass by a matching method of graph theory. *J. Phys. A: Math. and Gen.* **13** (1980), 2553–2576.
- [2] S. Boixo et al, Evidence for quantum annealing with more than one hundred qubits, *Nature Physics* **10** (2014), 218–224, previously (2013) <http://arxiv.org/abs/1304.4595>
- [3] A. Decelle and F. Krzakala, Belief-propagation-guided Monte-Carlo sampling, *Phys. Rev. B* **89** (2014), previously (2013) <http://arxiv.org/abs/1307.7846>
- [4] D-Wave Systems, Inc., The 128-qubit Rainier chip: II. graph embedding (2008), <http://dwave.wordpress.com/2008/10/23/the-128-qubit-rainier-processor-ii-graph-embedding/>
- [5] A. Fix, J. Chen, E. Boros, R. Zabih, Approximate MRF Inference Using Bounded Treewidth Subgraphs, *Lecture Notes in Computer Science* **7572** (2012) pp 385–398, also <http://www.cs.cornell.edu/~afix/Papers/ECCV12.pdf>
- [6] F. Hamze and N. de Freitas, From Fields to Trees, *Proceedings of the 20th Conference on Uncertainty in Artificial Intelligence* (AUAI Press, Arlington, Virginia, 2004), pp. 243–250. Also <http://www.cs.ubc.ca/~nando/papers/tree2.pdf>.
- [7] K. Hukushima, K. Nemoto, Exchange Monte Carlo Method and Application to Spin Glass Simulations (1995), <http://arxiv.org/abs/cond-mat/9512035>
- [8] S. V. Isakov, I. N. Zintchenko, T. F. Rønnow, M. Troyer, Optimized simulated annealing for Ising spin glasses (2014), <http://arxiv.org/abs/1401.1084>
- [9] H. Katzgraber, F. Hamze and R. Andrist, Glassy Chimeras could be blind to quantum speedup: Designing better benchmarks for quantum annealing machines (2014), <http://arxiv.org/abs/1401.1546>
- [10] H. Katzgraber, Exchange Monte Carlo: An efficient workhorse for optimization problems, http://www.physik.uni-leipzig.de/~janke/ENRAGE-School08/talks/Katzgraber_1.pdf
- [11] Rønnow et al (2014), Defining and detecting quantum speedup, <http://arxiv.org/abs/1401.2910>
- [12] A. Selby, QUBO-Chimera, Github repository (2013), <https://github.com/alex1770/QUBO-Chimera>

- [13] A. Selby, D-Wave: comment on comparison with classical computers (2013), <http://www.archduke.org/stuff/d-wave-comment-on-comparison-with-classical-computers/>
- [14] A. Selby, Harder QUBO instances on a Chimera graph (2013), <http://www.archduke.org/stuff/d-wave-comment-on-comparison-with-classical-computers/harder-qubo-instances-on-a-chimera-graph/>
- [15] A. Selby, D-Wave: scaling comparison with classical algorithms (2014), <http://www.archduke.org/stuff/d-wave-comment-on-comparison-with-classical-computers/d-wave-scaling-comparison-with-classical-algorithms/>
- [16] A. Selby, Efficient subgraph-based sampling of models with frustration (2014), <http://www.archduke.org/stuff/d-wave-comment-on-comparison-with-classical-computers/efficient-tree-based-sampling-of-models-with-frustration/>
- [17] U. Wolff, Collective Monte Carlo Updating for Spin Systems, *Phys. Rev. Lett.* **62** (1989), 361.